



CHORUS

This is the accepted manuscript made available via CHORUS. The article has been published as:

Resolving anomalous strain effects on two-dimensional phonon flows: The cases of graphene, boron nitride, and planar superlattices

Taishan Zhu and Elif Ertekin

Phys. Rev. B **91**, 205429 — Published 20 May 2015

DOI: [10.1103/PhysRevB.91.205429](https://doi.org/10.1103/PhysRevB.91.205429)

Resolving anomalous strain effects on two-dimensional phonon flows: the cases of graphene, boron nitride, and planar superlattices

Taishan Zhu, Elif Ertekin*

Department of Mechanical Science & Engineering, University of Illinois at Urbana Champaign, IL 61820

The physics of thermal transport on strained, 2D materials graphene, boron nitride, and their superlattices is analyzed by molecular dynamics, lattice dynamics, and numerical solutions to Boltzmann transport equation. The thermal conductivity of these materials is found to be highly sensitive to tensile strain, and the strain dependence itself is also highly dependent on the sample total length. Both finite-sized systems (varying from ~ 100 to 300 nm long) as well infinitely long systems are considered. In contrast to the typical reduction of thermal conductivity with strain exhibited by bulk 3D materials, the thermal conductivity initially increases to a peak value, after which it then decreases with further strain. Modal decomposition of the phonon spectrum shows that the non-monotonic behavior arises from a competition between in-plane softening and flexural stiffening of phonons. The length sensitivity arises from the nature of the linear/quadratic dispersion of the in-plane/flexural modes and their distinct scattering selection rules: longer systems favor out-of-plane flexural phonon stiffening while smaller systems favor in-plane phonon softening. Additionally, we show that this competition occurs in concert with a strain-induced transition in the nature of the phonon flow from ballistic-dominant to diffusive-dominant. Overall these effects give rise to a complex dependence of thermal conductivity on strain and sample size.

PACS numbers(s): 05.60.-k, 63.20.-e, 63.22.-m, 66.70.-f, 68.65.

I. INTRODUCTION

The class of two-dimensional materials including graphene, boron nitride, and their planar superlattices has received interest as a playground for nanoscale thermal engineering¹⁻². These materials exhibit rich thermal physics and potentially offer a route to tailored thermal properties.³ Through confinement of a material to one atomic plane, interesting phononic effects can arise. For example, flexural phonon modes emerge with unique characteristics such as parabolic (rather than linear) dispersion and peculiar selection rules governing their scattering.³ This leads to a crossover of thermal conductivity to that of 3D graphite when layers of graphene are stacked.⁴ The flexural modes are also intimately related to the recent debate regarding possible divergence of the thermal conductivity of graphene⁵⁻⁶. Furthermore, 2D superlattices of graphene and boron nitride have recently been studied, and sensitive dependences of thermal conductivity on superlattice period and interfacial defects have been reported⁷.

Amongst the many questions that remain regarding 2D materials, one question is how the presence of strain affects the thermal transport. On one hand, *ab initio* lattice dynamics simulations⁸ and classical equilibrium molecular dynamics simulations⁹ demonstrate that the thermal conductivity κ of unstrained graphene ultimately converges to a finite value as the sample size increases. However these simulations demonstrate not only that κ is enhanced when strain is present, but also that strain changes the asymptotic behavior of the length-dependence, yielding now a diverging κ . The change is attributed to the ZA flexural phonon modes: when unstrained, their vanishing group velocities contribute negligibly to conduction, but serve primarily as scattering pathways and prevent the logarithmic divergence predicted for purely 2D systems. According to these

analyses, strain ‘linearizes’ the normally parabolic dispersion of the ZA modes, and the increased group velocities then enable the ZA modes to contribute to conduction⁸⁻⁹.

Interestingly, these results are in sharp contrast with those of several non-equilibrium molecular dynamics simulations^{5,10-11}, which instead tend to find that (i) without the presence of strain, the κ of graphene may already diverge logarithmically as the system size increases⁵, and (ii) that the effect of strain for a fixed sample size is to reduce (rather than increase) κ .¹⁰⁻¹¹ Conventional wisdom based on what is known about bulk 3D materials supports the idea that in general tensile strains soften phonon modes, depress group velocities, and decrease relaxation times.¹² Additionally, even before strain is imposed, decomposition of κ into modal contributions suggests that the ZA modes contribute to (and may even be dominant contributors to) κ . However many of these studies have been carried out for single, finite-sized samples and the length-dependence of the reported trends is not clear. We have found one exception to this trend in the literature, which is an NEMD study of the effects of strain on silicene, a 2D allotrope of graphene, in which an increase in κ with strain is reported¹³.

In this work, we use several techniques (non-equilibrium molecular dynamics, equilibrium molecular dynamics, harmonic lattice dynamics, and the Boltzmann transport equation) to understand how strain influences thermal transport in 2D materials. We considered samples ranging from 100-300 nm using non-equilibrium molecular dynamics and the Boltzmann transport equation; further we use the latter to extend our analysis to infinite systems. The length-dependent analysis presented here offers an explanation for the above discrepancies. As the applied strain increases we find that graphene, boron nitride, and graphene/boron nitride superlattices generally become more thermally

conducting up to a threshold strain, beyond which κ begins to decrease. The non-monotonic behavior occurs as a result of a competition between stiffening of flexural ZA modes and softening of in-plane phonon modes. The position of the peak in κ , however, is highly sensitive to the total length: for reasons that we will discuss, the former effect is dominant in large systems, and the latter in small systems. Our analysis brings the seemingly disparate results reported above into concert. Further, we demonstrate that the application of strain induces a transition in the nature of the phonon flow from ballistic-dominant to diffusive-dominant. Overall these effects give rise to a complex dependence of κ on the applied strain and sample size for 2D materials.

II. MODEL STRUCTURES & COMPUTATIONAL METHODS

We consider three 2D systems: graphene (G), hexagonal boron nitride (BN), and planar graphene-boron nitride superlattices (G/BN). For example, FIG. 1(a) illustrates a G/BN superlattice composed of alternating graphene and boron nitride sections. We have implemented several different atomic-scale methods in our analysis: equilibrium and non-equilibrium molecular dynamics (EMD, NEMD), lattice dynamics (LD), and iterative solutions to Boltzmann transport equation (BTE). The EMD and NEMD simulations are implemented within LAMMPS¹⁴; we have used Tersoff potentials¹⁵ for G and BN as optimized by Lindsay and Broido¹⁶ for thermal properties. (For the case of the superlattice in which both carbon and boron/nitrogen atoms are present, Tersoff's mixing rules¹⁵ are applied to describe their interactions at superlattice interfaces). For the LD analysis that we use to spectrally decompose the heat carriers, we employed GULP¹⁷.

Finally, in order to evaluate scattering effects through numerical solution of the BTE solutions, we used the open-source package PhonTS¹⁸.

It is important to note that the different approaches used in our study introduce different levels of approximations. While LD truncates the spatial derivatives of the potential to second order (ignoring phonon-phonon scattering), it can still extract limited but useful harmonic information. By contrast, both molecular dynamics and the BTE account for phonon-phonon scattering, although in different manners. Within the BTE, the third derivatives of the energy are effectively incorporated *via* phonon relaxation times, and the resulting equations are solved numerically within a computational supercell¹⁸. On the other hand the classical molecular dynamics simulations incorporate anharmonic effects directly within the many-body potential.

In our EMD and NEMD simulations, periodic boundary conditions are always applied. We use a time step of 0.1 fs. All systems are initially relaxed and then thermalized for at least 10 ps with Nose-Hoover thermostats; the systems are considered to be thermalized when steady ensemble fluctuations around the target temperature $T = 300$ K have been established. In NEMD, the system is sandwiched between two heat baths as shown in FIG. 1(a). To mimic real world experiments, a quantity of heat Q is extracted from the cold bath and replenished to the hot bath. This procedure establishes a steady thermal gradient ΔT ,¹⁹ based on which the thermal conductivity can be estimated from Fourier's law $Q = -\kappa \Delta T$ (computational details of our NEMD approach are described in detail in Ref. 7). All molecular dynamics results reported are determined from a minimum of three independent simulations (each is run for at least 1 ns), and system averages are determined by binning quantities of interest to ensure statistically uncorrelated sampling;

all error bars denote 95% confidence intervals in the sampled quantity. In our NEMD simulations for finite systems, the computational domain is comprised of supercells with total lengths $L_0 = 300, 500,$ and 700 unit cells ($\sim 130, 215,$ and 300 nm respectively). As described below, the corresponding widths W are selected to maintain a constant aspect ratio. For the superlattice, a pitch of $P = 10$ unit cells (~ 4 nm) was selected; based on our previous work this is the pitch that minimizes the thermal conductivity⁷.

As always, with the use of NEMD²⁰, care must be taken to avoid spurious effects that may arise from the presence of heat baths and/or violation of the linear response regime. In our simulations, we have ensured that the induced temperature gradient is proportional to the heat flux so that linear response is not broken. Our choice of heat baths is based on the approach of Shiomi and Maruyama²¹, where the bath length is set to half of the system length L (we considered heat baths of different lengths, and find that our results are not substantially altered). A representative temperature profile was reported in our earlier work⁷, where no obvious effects due to thermal boundary resistance can be identified. We have also tested our results using baths made of different materials (*i.e.*, either G, or BN, or both), from which very stable thermal conductivities are obtained. Additionally, given the large aspect ratio of the finite-sized systems that we consider, care must also be taken to ensure that the calculated results are not unphysically large due to the quasi one-dimensional nature of the computational domain²². Therefore, FIG. 1(b) shows the results of a convergence test with respect to the width W for a system with total length $L_0 = 215$ nm: widths of $W = 12$ nm are well-converged, and thus this aspect ratio of 215:12 will be maintained for the remainder of our NEMD analysis.

To apply strain, materials of natural (unstrained) length L_0 are uniformly stretched in the longitudinal (x) direction to a length L . The total strain is defined as $\varepsilon_{xx} = (L - L_0)/L_0$. We exclusively study pristine crystals with strains less than 20%, which is close to the limit strain for graphene²³. As a result of the imposed strain, a stress σ_{xx} develops in the systems. FIG. 2(a) shows a typical stress distribution (shown here for the G/BN superlattice) as a function of the applied strain; as required by mechanical equilibrium σ_{xx} is continuous across the interfaces from the G to the BN subdomain. A snapshot of an atomic configuration is captured in FIG. 2(b) at $\varepsilon_{xx} = 15\%$, showing perfect crystalline interfaces and no resulting rips, tears, or other defects. We note that in our simulations, the width of the materials in the transverse direction is held fixed (rather than allowed to contract according to the Poisson ratio), resulting in the presence of smaller transverse stresses (σ_{yy}) as well. For several cases we checked the robustness of our results when transverse relaxations are allowed, and find that they are not substantially altered.

III. THERMAL CONDUCTIVITY OF FINITE SYSTEMS

UNDER TENSILE STRAIN

FIG. 3(a-c) compares κ obtained *via* both BTE and NEMD for G, BN, and G/BN as a function of the applied strain for systems of total length $L_0 = 215 \text{ nm}^*$. Here the BTE

* In comparison to experimental measurements of κ , the values reported here are low. Compare for instance our κ for unstrained graphene ($\sim 1500 \text{ W/mK}$) to measured values which range from 2000 to 5000 W/mK (see Ref. [1]). This underestimate is typical for simulations of finite sized samples for which the transport is largely ballistic. Moreover, discrepancies from experiment can be further aggravated by the use of an empirical potential, the neglect of quantum carrier statistics, and the introduction of boundary scattering. Our reported values however are in good agreement with other simulations of similarly sized samples (*e.g.* Refs. [5] and [9]).

results are obtained without including anharmonic scattering effects in the relaxation times: only boundary scattering $\tau = L/v$ for each phonon is incorporated. In comparison with silicene results previously reported also from NEMD¹³, the lattice conductivities of G, BN, and G/BN behave very differently. At small tensile strains, κ of graphene appears relatively insensitive (in NEMD the fluctuations are within error bars), while that of BN somewhat increases, and G/BN increases markedly. At larger applied strains, κ for all three systems starts decreasing. As plotted in FIG. 3(a-c), overall the κ from NEMD coincide well with those from BTE; the agreement is particularly good in the low-strain regime but exhibits some deviations at increasing strain (to be discussed later).

To compare the relative sensitivity of the three systems to strain, FIG. 3(d) shows the conductivities normalized by their respective unstrained values. Overall, the superlattice exhibits the greatest sensitivity, followed by BN, and then by G. At small strains, while κ of BN and G/BN increase with strain, G appears to be relatively strain-neutral (variations are within 5% of the unstrained value). For the superlattice, which is most sensitive, κ first increases up to strains $\varepsilon_{xx} \sim 7\%$ and then begins to decrease, giving a volcano shape. The non-monotonic response contrasts with the monotonically increasing trend reported for silicene¹³, and particularly contrasts starkly with the well-documented reduction of κ with tensile strain that is typically reported for NEMD simulations of 2D materials¹⁰⁻¹¹. We note that a similarly non-monotonic relationship was reported in Ref. 24, but in this case the initial increase was attributed to the relaxation of an initially buckled configuration. This explanation does not apply to our materials, which are initially completely equilibrated before application of strain. Furthermore, even at the

largest applied strains, we see no tears, holes, or other defects (FIG. 2 (b)) that might give rise to the observed behavior.

IV. TRANSPORT REGIMES

To explore the physics that gives rise to the non-monotonic dependence for the $L_o = 215$ nm, $W = 12$ nm systems in FIG. 3, it is helpful to establish the ballistic vs. diffuse nature of the phonon flows. This can be accomplished via the phononic Knudsen number, defined by $Kn = \Lambda/L_c$, where Λ and L_c are respectively the phonon mean free path and a system characteristic length. Strict limits to the nature of flows are typically given by $Kn > 10$ for ballistic flow and $Kn < 0.01$ for diffusive flow²⁵. While phonons carry heat and transfer energy between boundaries without inter-phonon collisions in the ballistic regime, they usually encounter multiple scattering events before delivering heat between boundaries in the diffusive regime. In the intermediate so-called ‘transitional’ regime (*i.e.*, $0.01 < Kn < 10$), both ballistic and diffusive natures coexist and compete. (We note that models such as non-equilibrium Green’s function (NEGF) and the Landauer formalism are rigorously valid when $Kn > 10$, although in practice many reported ballistic flows are actually in the transitional regime.) Moreover, such coexistence and competition can often give rise to intriguing transport phenomena²⁶.

To determine the nature of the flow for the $L_o = 215$ nm systems in FIG. 3, it is necessary to obtain an estimate of the phonon mean free path Λ . For this, we employed EMD to extract long-ranged and short-ranged phonon relaxation times²⁷. As suggested by previous studies (*e.g.* Refs. 10, 27 and references therein), the total κ can be decomposed

as $\kappa = \kappa_{sh} + \kappa_{lg}$, where κ_{sh} and κ_{lg} are contributions due to short-ranged and long-ranged phonons (corresponding loosely to diffuse and ballistic carriers respectively). These two phonon families are characterized by their distinct relaxation times τ_{sh} and τ_{lg} , which are extracted by fitting the heat flux auto-correlation function (HFACF) to the functional form $C_{yy}(t) = A_1 e^{-t/\tau_{sh}} + A_2 e^{-t/\tau_{lg}}$ as shown in the inset of FIG. 4(a) for a G/BN superlattice. While τ_{sh} is reported to be insensitive to temperature and strain, the long-ranged carriers are believed to respond sensitively and account for the temperature dependence of thermal conductivity.²⁷ We find a similar trend as shown in FIG. 4(a): the short-ranged phonon relaxation time stays relatively constant for all strains (~ 0.2 ps), while the relaxation time for the long-ranged phonons drops monotonically from ~ 4 ps to ~ 0.2 ps as the strain increases. This drop indicates a change in the nature of the flow from more ballistic-like towards more diffusive-like.

Using the relaxation times of FIG. 4(a), a representative Knudsen number for the long-ranged flow can now be estimated by $Kn = \Lambda_p/L_c$, where $\Lambda_p = v_p\tau_{lg}$, v_p is the longitudinal sound speed, and $L_c = L$. The Knudsen number of long-ranged longitudinal phonons for G/BN is illustrated in FIG. 4(b) as a function of strain. For the unstrained system $Kn \sim 15$ (strictly ballistic flow); as the strain increases Kn decreases monotonically to $Kn \sim 0.4$ (although not shown here explicitly, the pure graphene and BN systems exhibit similar trends). This observed change in Kn is consistent with the deviation between MD and BTE results in FIG. 3. Since inter-phonon collisions are not accounted for in the BTE analysis, the two techniques give similar results at small strains where collisions are not significant, but deviate somewhat from each other at larger strain where phonon collisions are enhanced.

It is also interesting to note that for the majority of cases considered, the phonon flows are located in the transitional regime. Nevertheless, as the strain increases, the nature of the flow changes from ballistic-dominant towards diffusive-dominant. Although it is difficult to determine the precise physical mechanism underpinning the decrease of Kn , it is feasible that it arises from the softening of bonds when tensile strain is applied (discussed later), which can introduce inter-phonon scattering and reduce mean free paths^{12,24}.

V. SPECTRAL DECOMPOSITION

To further provide insights to the strain dependence of κ , we decomposed the total κ into contributions from distinct phonon families for the systems shown in FIG. 3. In the Boltzmann framework, the total lattice conductivity is given by

$$\kappa(T, \varepsilon) = L \sum_{\chi} \int_0^{\infty} \frac{1}{(2\pi)^2} v_{\omega, \chi} C_{\omega, \chi} g(\omega, \varepsilon) d\omega \quad (1)$$

where $g(\omega, \varepsilon)$ denotes phonon density of states, $v_{\omega, \chi} = \partial\omega_{\chi}/\partial k_{\chi}$ and $C_{\omega, \chi} = k_B x^2 e^x (e^x - 1)^{-2}$ are respectively the modal group velocity and heat capacity, k_B denotes the Boltzmann constant, $x = \hbar\omega/k_B T$, and χ denotes a summation over phonon branches. The parameters in Eq. (1) such as the DOS, group velocity, *etc.*, are obtained with lattice dynamics (LD).

Figure 5(a-c) shows the phonon dispersion spectrum from LD for G, BN, and G/BN under various strains, where the acoustic branches are labeled according to their character: LA (longitudinal acoustic), TA (transverse acoustic), and ZA (out-of-plane

acoustic). As shown in FIG 5(a-c), a competition between softening of the LA modes and a stiffening of the ZA modes occurs as the applied strain increases (indicated by the arrows). This manifests as a drop in the LA frequencies and an increase in the ZA frequencies (and corresponding changes to their group velocities). Take BN for example: the sound speed of the LA modes is reduced by $\sim 1\%$ at 10% applied strain, and $\sim 17\%$ at 15% applied strain. Meanwhile, the ZA mode group velocity is enhanced by a factor of ~ 7.5 and ~ 9 for the same strains, respectively. Particularly notable is that the change observed in the ZA modes represents not only a stiffening, but is also associated with a change from parabolic dispersion (vanishing group velocity at the zone center) to a linear dispersion (non-vanishing group velocity at the zone center). This ‘linearization’ has been observed previously in *ab initio* LD⁸ and EMD simulations⁹. (In comparison to the behavior of the LA and ZA modes, FIG. 5(a-c) shows that the TA modes here appear less sensitive to the application of strain.)

In FIG. 5(d-f), we decomposed the total κ in Eq. (1) into contributions summed individually over the different phonon families. This decomposition shows that before strain is applied, the contribution of the planar modes is larger than that of the flexural modes (at least for this system size). It also quantitatively shows however that the contribution of the ZA modes increases with tensile strain, while that of the LA modes decreases. We also find that this analysis of the LA, TA, and ZA contributions at different applied strains can reproduce the non-monotonic trends in FIG. 3. For instance, for G/BN, by summing the total contribution over all modes, the maximum enhancement in κ of the superlattice is 32.9% and occurs at a strain of 7%, which is in very close agreement to NEMD results in FIG. 3(c). (Note that there are some differences in the

magnitude of κ , since the LD results do not include scattering and in general are expected to give larger thermal conductivities).

VI. EFFECT OF TOTAL SYSTEM LENGTH

The results presented thus far correspond to G, BN, and G/BN systems with total length $L_o = 215$ nm. It is necessary to consider how the trends may vary for systems of different size. The length-dependence of the strain response is expected to be non-trivial, given the competing role of strain in both softening in-plane modes, while stiffening and linearizing flexural modes. Since the nature of the transport in our systems ranges from ballistic to transitional, as the total sample length increases the contributions to κ of longer wavelength phonon modes (both in-plane and out-of-plane) will increase accordingly; however, in addition the affect of the applied strain on the modal contributions must also be ascertained.

To analyze how our results change for different lengths L_o , we carried out NEMD simulations of thermal conductivity *vs.* strain for a 2D G/BN superlattice now with total lengths $L_o = 130$ and 300 nm to compare to the previous result with $L_o = 215$ nm. We chose the superlattice because it exhibited the largest strain sensitivity, and provides the best opportunity to probe the mechanism underlying the response. FIG. 7 shows a comparison of the results for the different sizes. As expected, regardless of strain κ is always larger for the longer systems. The non-monotonic response is maintained for all systems. However, two additional trends are present. First, larger system size amplifies

the initial increase in κ (the slope of the curve is larger). Second, for larger systems, the onset of the turn around is delayed (*i.e.* the peak appears at larger strain).

We attribute both of these observations to the nature of the (i) dispersion and (ii) scattering for the LA and ZA families. Regarding (i): before strain is applied, as sample length increases we expect that the effect of ZA modes on κ should be more pronounced than that of the LA modes, due to the quadratic dispersion and infinite density of states of the former. (Relatedly, in EMD simulations⁹ the contribution to κ of in-plane acoustic modes has been shown to converge relatively fast with system size, whereas the contribution arising from the ZA modes requires much larger simulation cells). When the sample is strained, these ZA modes become contributing carriers due to the linearization of their dispersion, resulting in a pronounced increase in κ . Regarding (ii), it is possible that the positive contribution to κ of the ZA modes may be even further enhanced by the selection rules that prevent their scattering^{1,3} and allow them to remain ballistic carriers. (Note however that when strain is applied, since the dispersion of the ZA modes becomes linearized, the special selection rule that prevents them from being scattered will gradually be destroyed.)

Based on these considerations, it is reasonable that in FIG. 7 the larger systems ($L = 300$ nm) in which the effects of the zone center ZA modes (and their stiffening/linearization) are better captured show a more pronounced increase in κ with strain, and a delayed onset of the turn around. Correspondingly for smaller sizes ($L_o = 130$ nm), the effects of ZA mode linearization cannot be fully realized so the softening of the LA modes dominates the response: as strain is applied these systems show only a modest initial increase in κ , which quickly turns over into a more pronounced reduction.

This explains the observed length dependence of the system's response to strain. Additionally, this length-sensitivity also explains the difference between previous EMD⁹ and *ab initio* LD results⁸ (carried out for more macroscopic systems and show increasing κ with strain) and the typical NEMD results¹⁰⁻¹¹ (which often report reduction in κ , but have been carried out for smaller systems a few 10's of nm for which the initial enhancement is completely suppressed). Indeed, the only NEMD result that reports an increase in κ with strain (silicene¹³) was also carried out for relatively large sample size (~687 nm).

To test further this analysis, BTE solutions enable predictions for systems that are infinite in size. In FIG. 8 we present a comparison of the strain effects on finite ($L = 215$ nm) and infinite G and BN. For the infinite systems, the mean free paths are obtained using iterative BTE solutions so that inherent phonon mean free paths are used to calculate κ directly. Similar to the comparison between finite G/BN of different lengths (FIG. 7), the larger (infinite) systems (dashed lines) exhibit a more pronounced initial increase in κ . Moreover, at infinite length, a slight enhancement of κ at small strains can also be identified even for pure G, before it again begins to decrease.

Before concluding, we consider possible reasons for the differences in the relative sensitivity of κ of G, BN, and G/BN to strain. In FIG. 3, the superlattice exhibited the largest sensitivity, while graphene was least sensitive. In both cases, as strain is applied, the softening of the in-plane modes gives a decreasing contribution to κ while the linearization of the ZA modes gives an increasing contribution: the question then is which effect is most dominant. In graphene, the in-plane modes have large group velocities and their relative contribution to total κ is very dominant. Thus, LA mode

softening has a comparatively large influence on κ , sufficient to offset the effects of ZA mode linearization. By contrast, in the superlattice even before strain is applied the planar modes are already substantially softened due to the superlattice itself structure (interfaces); their overall relative contribution to κ is lower to begin. Therefore, their softening with strain has a relatively smaller effect, allowing the linearization of the ZA modes to dominate the response.

VII. CONCLUSIONS

In summary, in this work we demonstrate that the strain-dependent thermal conductivity of 2D materials exhibits anomalous features arising from the competition between out-of-plane flexural stiffening and in-plane longitudinal softening. These features include a non-monotonic dependence of the thermal conductivity on the applied strain, which is highly sensitive to the total system size. We show that the nature of the phonon flow, which is initially ballistic for the strain-free samples, changes to the transitional flow regime as an external strain is applied. Our analysis helps to resolve discrepancies between previous results presented in the literature. Moreover, we note that the length-dependent NEMD predictions presented here can in principal be verified directly by experiment.

ACKNOWLEDGEMENTS

We are grateful to D. Donadio for valuable and insightful discussions. We also acknowledge A. Chernatynskiy for valuable discussions regarding the BTE calculations. This work is supported by the National Science Foundation through Grant No. CBET-1250192. Various computational resources were used in this work: this research is part of the Blue Waters sustained-petascale computing project, which is supported by the National Science Foundation (awards OCI-0725070 and ACI-1238993) and the state of Illinois. Blue Waters is a joint effort of the University of Illinois at Urbana-Champaign and its National Center for Supercomputing Applications. Additional resources were provided by (i) the Extreme Science and Engineering Discovery Environment (XSEDE) allocation DMR-140007, which is supported by National Science Foundation grant number ACI-1053575, and (ii) the Illinois Campus Computing Cluster.

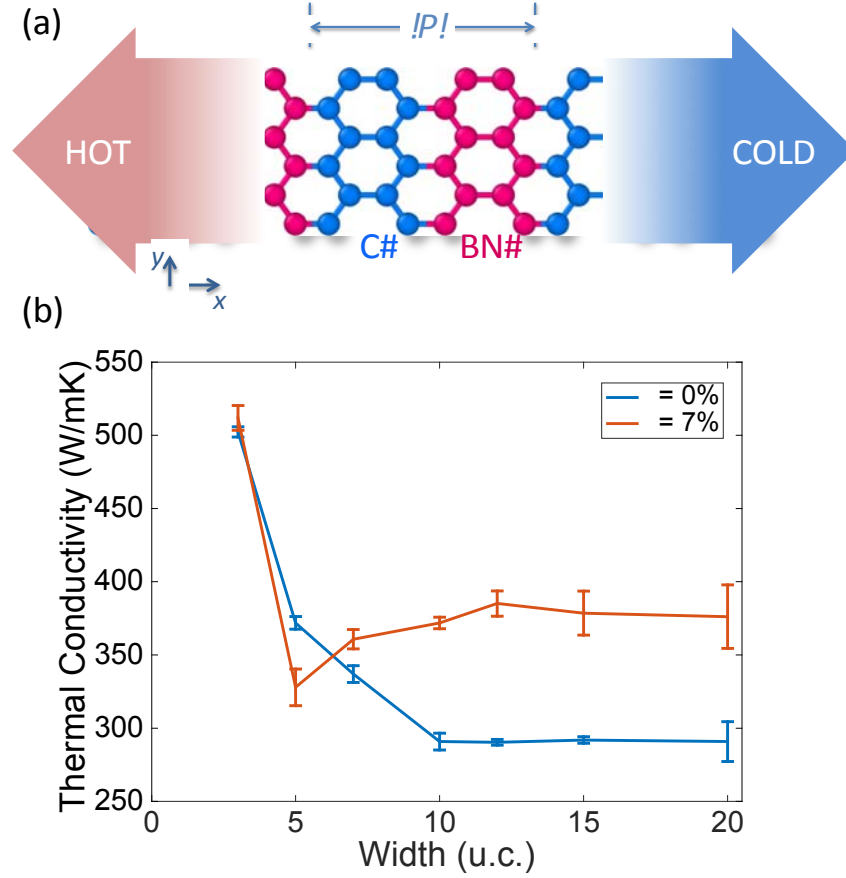


FIG. 1. (a) Schematic of a G/BN superlattice with strain $\epsilon = 15\%$. P denotes the superlattice period and L is the total length. Tensile strain is applied along the x -direction and meanwhile the superlattice sample is sandwiched between two heat baths for NEMD simulations. (b) The convergence of thermal conductivity of G/BN with varying widths W , for sample length $L = 215$ nm, both strained and unstrained.

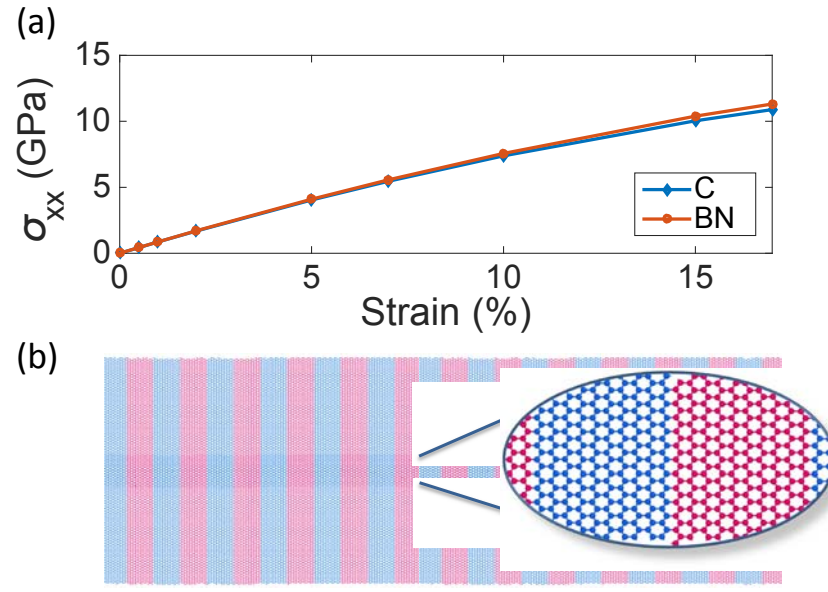


FIG. 2. (a) Longitudinal stresses σ_{xx} on G and BN subdomains of the G/BN superlattice as a function of applied strain. (b) A snapshot of atomic configuration at $\varepsilon = 15\%$, showing that no tears or rupturing occurs; the strain is accommodated homogeneously throughout the superlattice.

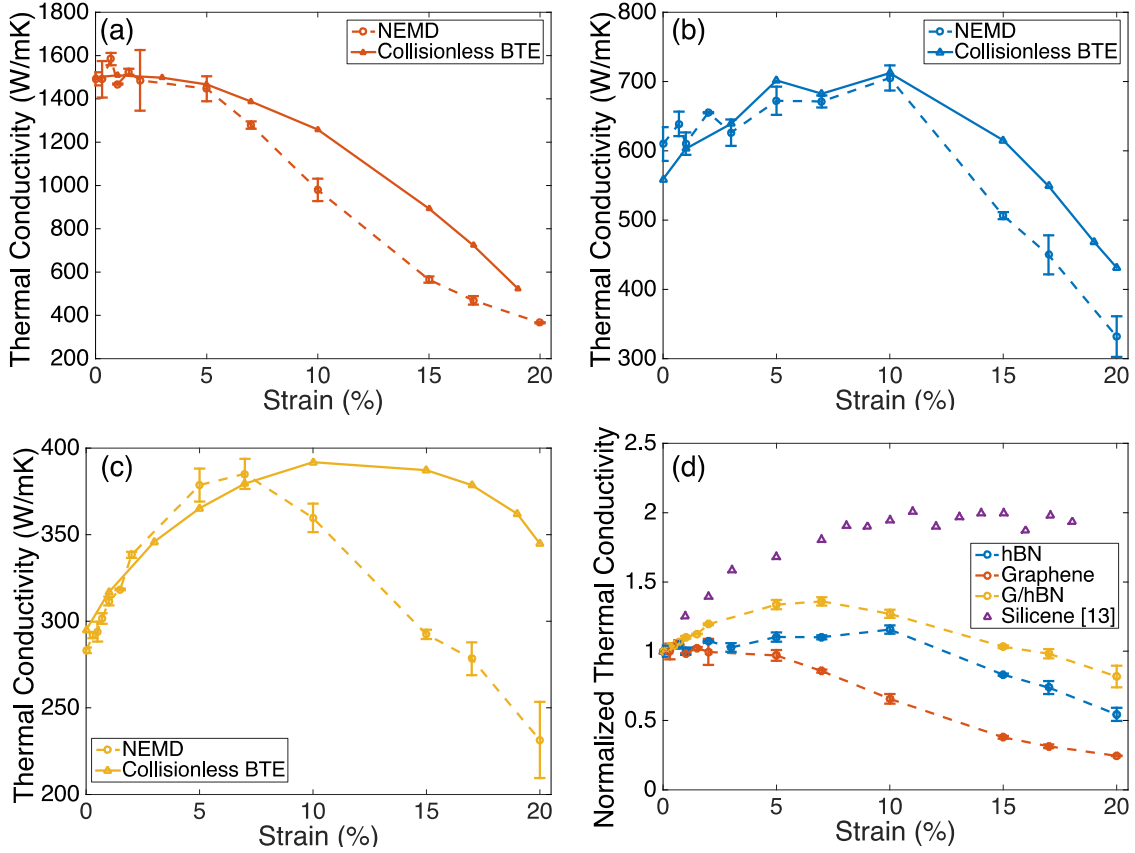


FIG. 3. Thermal conductivity vs. strain for (a) graphene, (b) boron nitride, and (c) G/BN superlattices, all with total length $L_o = 215$ nm. The solid lines represent numerical BTE calculations, while the dashed lines indicate NEMD results. While graphene is initially insensitive to strain, BN and G/hBN become increasingly conducting under small strains; for all systems the conductivity then decreases under large strain. In (d), the NEMD results are normalized to compare the relative sensitivities of all systems, and for comparison to previously reported results for silicene.

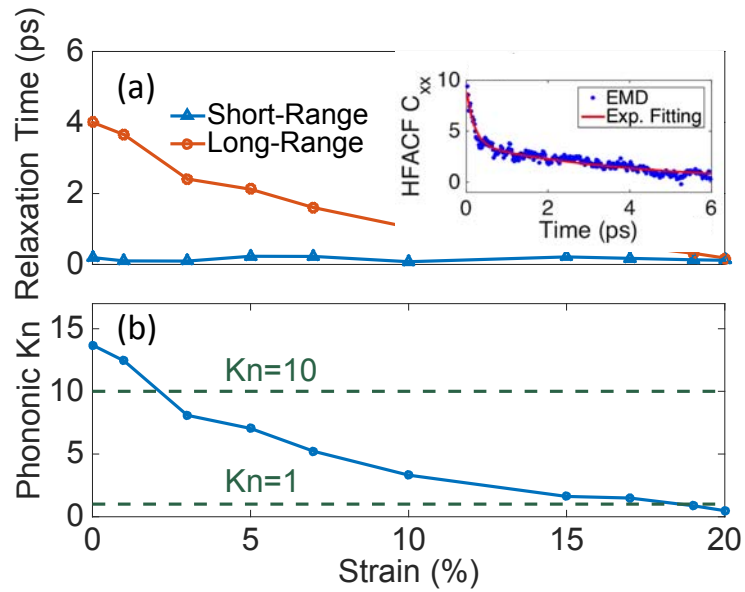


FIG. 4. (a) Long-ranged and short-ranged phonon relaxation times obtained by fitting heat flux autocorrelation functions (as shown in the inset), and (b) longitudinal Knudsen number of long-ranged relaxation times vs. tensile strain for the $L_o = 215$ nm superlattice. All strained phononic flows turn out to be in the transitional regime. As the strain is increased, the reduction of the Knudsen number indicates that transport becomes more diffusive-like.

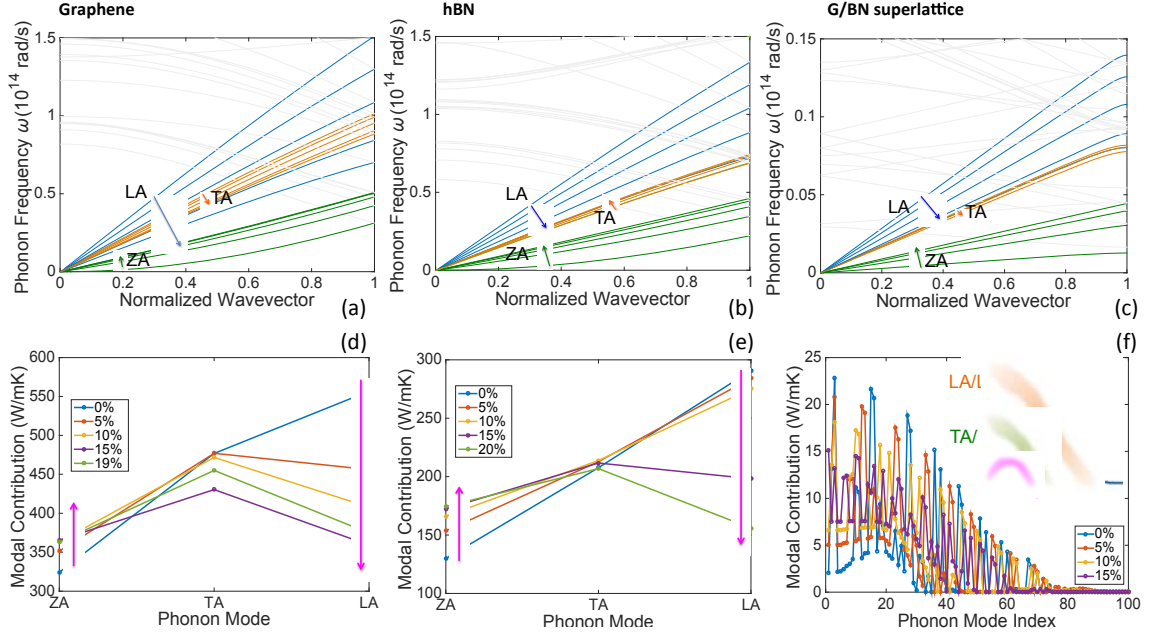


FIG. 5. (a-c): The phonon spectrum of (a) G, (b) BN, and (c) G/BN demonstrate that increased strain leads to reduced frequencies of LA modes and increased frequencies of ZA modes, while TA modes remain almost unchanged. The arrows indicate the trends for increasing strain, and the colors denote different mode families: blue (LA), orange (TA), and green (ZA). (d-f): The spectral decomposition for the three systems respectively shows the competition between LA and ZA modes. Here colors indicate the applied strain. Note that in (f) mode family differentiation has not been carried out for G/BN due to multiple zone folding, but the modes are approximately categorized by their relative contributions as indicated in the inset. In all cases, while the ZA contribution increases with strain, the LA contribution decreases. The competition between LA softening and ZA stiffening accounts for the variations of overall thermal conductivities.

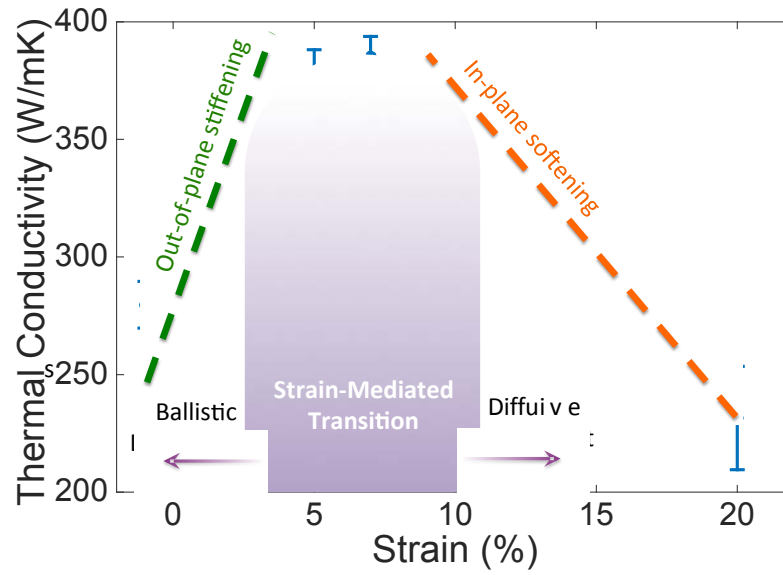


FIG. 6. Schematic illustration of strain dependence, in this case for G/BN. Strain facilitates the crossover from ballistic-dominant to diffusive-dominant transport of long-ranged phonons. These two regimes are, respectively, dominated by flexural mode stiffening and longitudinal mode softening.

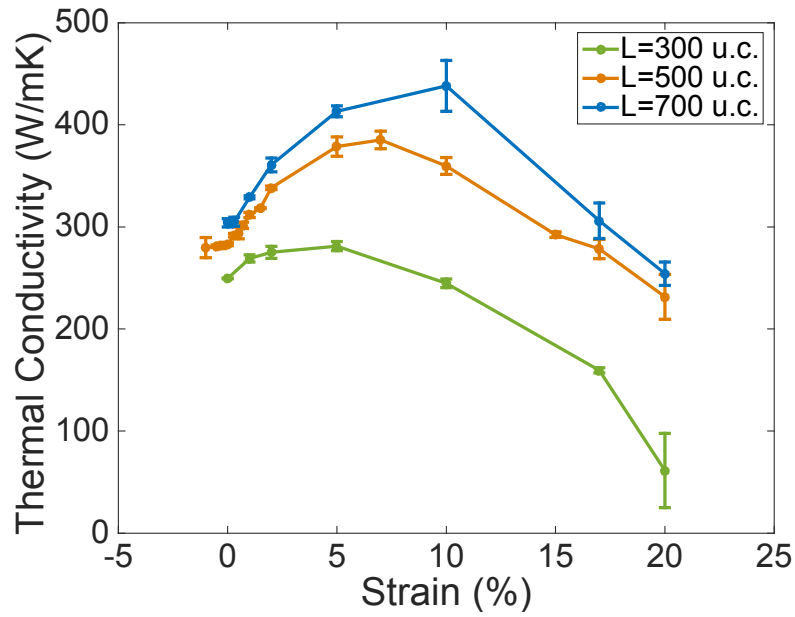


FIG. 7. Thermal conductivity of G/BN with different total lengths ($L=130, 215,$ and 300 nm). For all strains, as L increases, so does κ . Additionally, as L increases, both (i) the initial increase of κ vs. strain becomes more pronounced, and (ii) the peak occurs at larger strains.

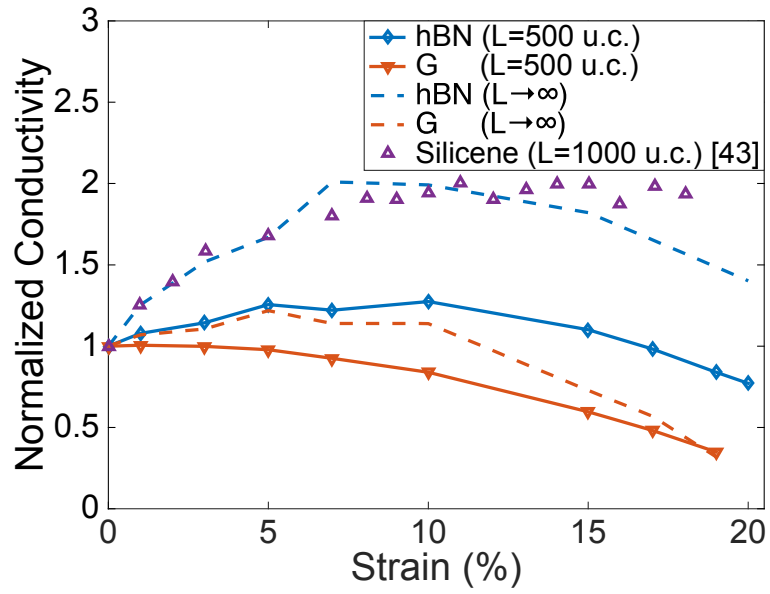


FIG. 8. Thermal conductivity of representative finite ($L_o = 215$ nm) and infinite G and BN obtained from BTE solutions, compared with previous silicene results. The infinite systems respond more sensitively than the corresponding finite systems to strain: they again show a more pronounced increase, and a delay in the onset of the turn around.

* Corresponding author: ertekin@illinois.edu

REFERENCES

- ¹ A. A. Balandin, *Nat. Mater.* **10**, 569 (2011).
- ² F. Bonaccorso, L. Colombo, G. Yu, M. Stoller, V. Tozzini, A. C. Ferrari, R. S. Ruoff, and V. Pellegrini, **347**, 6217 (2015).
- ³ A. A. Balandin and D. L. Nika, *Mater. Today* **15**, 266 (2012).
- ⁴ S. Ghosh, W. Bao, D. L. Nika, S. Subrina, E. P. Pokatilov, C. Ning Lau and A. A. Balandin, *Nat. Mater.* **9**, 555 (2010).
- ⁵ X. Xu, L. F. C. Pereira, Y. Wang, J. Wu, K. Zhang, X. Zhao, S. Bae, C. T. Bui, R. Xie, J. T. L. Thong, B. H. Hong, K. P. Loh, D. Donadio, B. Li, and B. Özyilmaz, *Nat. Comm.* **5**, 1 (2014).
- ⁶ D. L. Nika, A. S. Askerov, and A. A. Balandin, *Nano Lett.* **12**, 3238 (2012); M. Park, S. C. Lee, and Y. S. Kim, *J. Appl. Phys.* **114**, 053506 (2013).
- ⁷ T. Zhu, and E. Ertekin, *Phys. Rev. B* **90**, 195209 (2014).
- ⁸ N. Bonini, J. Garg, and N. Marzari, *Nano Lett.* **12**, 2673 (2012).
- ⁹ L. F. C. Pereira and Davide Donadio, *Phys. Rev. B* **87**, 125424 (2013).
- ¹⁰ X. Li, K. Maute, M. L. Dunn, and R. Yang, *Phys. Rev. B* **81**, 245318 (2010).
- ¹¹ N. Wei, L. Xu, H. Q. Wang, and J. C. Zheng, *Nanotechnology* **22**, 105705 (2011).
- ¹² K. D. Parrish, A. Jain, J. M. Larkin, W. A. Saidi, and A. J. H. McGaughey, *Phys. Rev. B* **90**, 235201 (2014).

- ¹³ M. Hu, X. Zhang, and D. Poulikakos, Phys. Rev. B **87**, 195417 (2013).
- ¹⁴ S. Plimpton, J. Comp. Phys. **117**, 1 (1995); <http://lammps.sandia.gov>
- ¹⁵ J. Tersoff, Phys. Rev. B **37**, 6991 (1988); **39**, 5566 (1989).
- ¹⁶ L. Lindsay and D. A. Broido, Phys. Rev. B **81**, 205441 (2010); **84**, 155421 (2011).
- ¹⁷ J. D. Gale and A. L. Rohlfing, Mol. Simulat. **29**, 291 (2003).
- ¹⁸ A. Chernatynskiy and S. R. Phillpot, Phys. Rev. B **82**, 134301 (2010).
- ¹⁹ T. Ikeshoji and B. Hafskjold, Mol. Phys. **81**, 251 (1994).
- ²⁰ R. N. Salaway, L. V. Zhigilei, Int. J. Heat Mass Trans. **70**, 954 (2014).
- ²¹ J. Shiomi, S. Maruyama, Jpn. J. Appl. Phys. **47**, 2005 (2008).
- ²² L. Hu, W. J. Evans, and P. Keblinski, J. Appl. Phys. **110**, 113511 (2011).
- ²³ X. Zhai and G. Jin, EPL **96**, 16002 (2011).
- ²⁴ Q. X. Pei, Y. W. Zhang, Z. D. Sha, and V. B. Shenoy, J. Appl. Phys. **114**, 033526 (2013).
- ²⁵ G. A. Bird, *Molecular Gas Dynamics and The Direct Simulation of Gas Flows* (Oxford: Clarendon Press, 1994).
- ²⁶ T. Zhu, and W. Ye, Phys. Rev. E **82**, 036308 (2010); T. Zhu, W. Ye, and J. Zhang, Phys. Rev. E **84**, 056316 (2011).
- ²⁷ A. J. H. McGaughey, and M. Kaviany, Int. J. Heat Mass Trans. **47**, 1783 (2004); B. Wolfing, C. Kloc, J. Teubner, E. Bucher, Phys. Rev. Lett. **86**, 4350 (2001).